Common-path laser planar encoder

Chyan-Chyi Wu,[1*] Yan-Zou Chen,[1,2] and Chia-Huang Liao[1]

[1]*Department of Mechanical and Electro-mechanical Engineering, Tamkang University, Taiwan*
[2]*Institute of Mechanical Engineering, National Taiwan University, Taiwan*
[*]*chyanchyi@gmail.com*

Abstract: This paper presents a common-path laser planar encoder (CLPE) for displacement measurements in the X- and Y- axes. The CLPE can effectively reduce the environmental disturbance to its lowest level. The experimental results of the CLPE match well with those of HP5529A for both short and long ranges. The CLPE can measure 2D displacement with high resolutions of 0.07 ± 0.021 nm and 0.07 ± 0.023 nm in the X- and Y- axes and also presents high system stabilities of –0.59 ± 0.43 nm/h and –0.63 ± 0.47 nm/h respectively in the X- and Y- axes. The CLPE has promising potential for nanometer resolution and large-range applications.

©2013 Optical Society of America

OCIS codes: (120.0120) Instrumentation, measurement, and metrology; (120.3180) Interferometry.

References and links

1. C. C. Wu, J. S. Yang, C. Y. Cheng, and Y. Z. Chen, “Common-path laser encoder,” Sens. Actuat. A **189**, 86–92 (2013).
2. P. L. M. Heydemann, “Determination and correction of quadrature fringe measurement errors in interferometers,” Appl. Opt. **20**(19), 3382–3384 (1981).
3. J. D. Ellis, M. Baas, K.-N. Joo, and J. W. Spronck, “Theoretical analysis of errors in correction algorithms for periodic nonlinearity in displacement measuring interferometers,” Precis. Eng. **36**(2), 261–269 (2012).
4. W.-W. Chiang and C.-K. Lee, “Wavefront reconstruction optics for use in a disk drive position measurement system,” USPTO, ed. (International Bussiness Machines, America, 1995).
5. V. V. Yashchuk, “Optimal measurement strategies for effective suppression of drift errors,” Rev. Sci. Instrum. **80**(11), 115101 (2009).
6. C.-M. Wu and R. D. Deslattes, “Analytical modeling of the periodic nonlinearity in heterodyne interferometry,” Appl. Opt. **37**(28), 6696–6700 (1998).
7. W. Gao, T. Araki, S. Kiyono, Y. Okazaki, and M. Yamanaka, “Precision nano-fabrication and evaluation of a large area sinusoidal grid surface for a surface encoder,” Precis. Eng. **27**(3), 289–298 (2003).
8. W. Gao, S. Dejima, H. Yanai, K. Katakura, S. Kiyono, and Y. Tomita, “A surface motor-driven planar motion stage integrated with an $XY\theta_Z$ surface encoder for precision positioning,” Precis. Eng. **28**(3), 329–337 (2004).
9. W. Gao, S. Dejima, and S. Kiyono, “A dual-mode surface encoder for position measurement,” Sens. Actuat. A **117**(1), 95–102 (2005).
10. W. Gao and A. Kimura, “A three-axis displacement sensor with nanometric resolution,” CIRP Annals - Manufacturing Technology **56**(1), 529–532 (2007).
11. A. Kimura, W. Gao, A. Yoshikazu, and L. Zeng, “Design and construction of a two-degree-of-freedom linear encoder for nanometric measurement of stage position and straightness,” Precis. Eng. **34**(1), 145–155 (2010).
12. A. Kimura, W. Gao, and L. Zeng, “Position and out-of-straightness measurement of a precision linear air-bearing stage by using a two-degree-of-freedom linear encoder,” Meas. Sci. Technol. **21**(5), 054005 (2010).
13. A. Kimura, W. Gao, W. Kim, K. Hosono, Y. Shimizu, L. Shi, and L. Zeng, “A sub-nanometric three-axis surface encoder with short-period planar gratings for stage motion measurement,” Precis. Eng. **36**(4), 576–585 (2012).
14. X. Li, W. Gao, H. Muto, Y. Shimizu, S. Ito, and S. Dian, “A six-degree-of-freedom surface encoder for precision positioning of a planar motion stage,” Precis. Eng. **37**(3), 771–781 (2013).
15. C. F. Kao, S. H. Lu, and M. H. Lu, “High resolution planar encoder by retro-reflection,” Rev. Sci. Instrum. **76**(8), 085110 (2005).
16. Y.-C. Chung, K.-C. Fan, and B.-C. Lee, “Development of a novel planar encoder for 2D displacement measurement in nanometer resolution and accuracy,” in *Intelligent Control and Automation (WCICA), 2011 9th World Congress on*(2011), pp. 449–453.
17. H.-L. Hsieh, J.-C. Chen, G. Lerondel, and J.-Y. Lee, “Two-dimensional displacement measurement by quasi-common-optical-path heterodyne grating interferometer,” Opt. Express **19**(10), 9770–9782 (2011).

#190296 - $15.00 USD Received 5 Jun 2013; revised 4 Jul 2013; accepted 5 Jul 2013; published 1 Aug 2013

18. J.-Y. Lee, H.-L. Hsieh, G. Lerondel, R. Deturche, M.-P. Lu, and J.-C. Chen, “Heterodyne grating interferometer based on a quasi-common-optical-path configuration for a two-degrees-of-freedom straightness measurement,” Appl. Opt. **50**(9), 1272–1279 (2011).
19. K. C. Fan, B. H. Liao, Y. C. Chung, and T. T. Chung, “Displacement measurement of planar stage by diffraction planar encoder in nanometer resolution,” in *2012 IEEE International Conference on Instrumentation and Measurement Technology*(2012), pp. 894–897.
20. C.-C. Hsu, M.-C. Kao, K.-C. Huang, and C.-C. Wu, “Reflection type displacement sensor with volume hologram for in-plane displacement measurement,” in *2012 International Conference on Measurement, Information and Control (MIC)* (2012), pp. 13–16.
21. C.-C. Wu, C.-H. Liao, Y.-Z. Chen, and J.-S. Yang, “Common-path Laser Encoder with Littrow Configuration,” Sens. Actuat. A **193**, 69–78 (2013).
22. R. Petit and L. C. Botten, *Electromagnetic Theory of Gratings* (Springer-Verlag, 1980).
23. L. E. Drain, *The Laser Doppler Technique* (John Wiley, 1980).
24. *http://www.newport.com*.
25. C.-F. Kao, C. C. Chang, and M.-H. Lu, “Double-diffraction planar encoder by conjugate optics,” Opt. Eng. **44**(2), 023603 (2005).
26. F. L. Pedrotti, L. M. Pedrotti, and L. S. Pedrotti, *Introduction to Optics* (Prentice-Hall International, 2006).
27. http://www.piezosystem.com/home/.
28. P. Gregorcic, T. Pozar, and J. Mozina, “Quadrature phase-shift error analysis using a homodyne laser interferometer,” Opt. Express **17**(18), 16322–16331 (2009).
29. Sony Precision Technology, *http://www.sonypt.com/*.

1. Introduction

Two-dimensional (2D) or planar displacement measurements play an important role in precision equipment of a variety of scientific and technology fields, such as scanning probe microscopes (SPM), scanning electron microscopes (SEM), stepping lithographers, and so on. Subnanometer resolution, long-range measurement, and high throughput are all necessary for this coming technology node. For subnanometer resolution and long-range measurement, the noise level and drift of a measurement system must be small enough. Practically, displacement drift error in a measurement system is frequently more than hundreds of nm per hour [1]. Note that the error contribution of drift generally cannot be averaged out using a number of measurements identically carried out over a reasonable time [2–5]. In addition, environmental disturbances, including temperature, pressure, and humidity variations, as well as vibrations from the base and foundation, directly contribute an additional phase change to the interference signals. The displacement error from such an additional phase change can rise to the micron range, which can be about three orders of magnitude greater than those errors from optics nonlinearity [6]. However, such an additional phase change in laser encoders and laser interferometers cannot be effectively corrected through software or electronic processing. Thus, the error from environmental disturbances is the barrier to subnanometer resolution in a displacement measurement system.

Many publications over the past decade have studied planar laser encoders [7–20]. Gao et al. studied a series of surface encoders for measurement of in-plane X- and Y-displacements as well as yaw and out-of-plane motions. These surface encoders capable of multi-axial measurements concentrated on the error measurements in precision stages and CNC machine tools [7–14]. Kao et al. reported a homodyne planar laser encoder with an optical configuration of four symmetric 1-x telescopes [15]. The measurement resolution of the planar laser encoder was 1 nm under an electronic interpolation with a factor of 400. A circular motion experiment indicated that the motion deviation of the planar encoder was less than 30 nm and the repeatability was better than 8 nm. Chung et al. proposed a planar diffraction grating interferometer (PDGI) [16]. The PDGI combined two independent sets of linear diffraction grating interferometers (LDGIs) having independent optical paths and laser sources. Its measurement errors in the X- and Y- directions were better than 20 nm for a 25-mm range in a common laboratory environment. Hsieh et al. presented a 2D quasi-common-path heterodyne grating interferometer (QCOP) for X- and Y- displacement measurements in the few-millimeter range [17]. Two types of 2D QCOPs were investigated. The corresponding measurement resolutions could be estimated to be 1.41 and 2.52 nm

#190296 - $15.00 USD Received 5 Jun 2013; revised 4 Jul 2013; accepted 5 Jul 2013; published 1 Aug 2013
(C) 2013 OSA

respectively. Lee et al. also studied 2D QCOP for 2D displacement and straightness measurements [18]. It achieved a system resolution and stability of 1.3 nm and 40 nm, respectively, within a 30-min measurement. In the above-mentioned publications, only Hsieh et al. and Lee et al. considered the problem of environmental disturbances.

In our previous work, we demonstrate a common-path laser encoder (CPLE) for one-dimensional displacement measurement [1]. However, the CPLE cannot measure 2D displacements and geometrical errors of a precision stage. This paper extends the CPLE configuration and presents a planar common-path laser encoder (CLPE) for 2D displacement measurements. The CLPE can effectively reduce the effect from environmental disturbances. The measurement principle and the runout tolerance are detailed. Experiments for short- and long-range measurements are performed. The experimental results demonstrate that the CLPE not only can measure 2D displacement with high resolutions of 0.07 ± 0.021 nm and 0.07 ± 0.023 nm in the X - and Y - axes, but also presents high system stabilities of –0.59 ± 0.43 nm/h and –0.63 ± 0.47 nm/h respectively in the X - and Y - axes. The CLPE has a promising potential for displacement measurements in 2D subnanometer positioning.

2. Principle

A 2D grating scale is installed and fixed on the base of a moving stage. The optical read-head of the CLPE is installed on the moving platform of the moving stage. The optical configuration of the CLPE is shown in Fig. 1. Actually, there are two common-path configurations in the CLPE readhead [21]. One configuration is for the X -displacement, and the other one is for the Y -displacement. A laser beam passes through a Fresnel lens and is focused on a two-dimensional grating scale, with the focal point on the grating scale. The grating scale diffracts the focused laser beam and builds up a three-dimensional (3D) diffraction, with the two-dimensional diffraction orders represented by (m , n), where m and n are integers. The interference between the (0, 0) and (1, 0) order diffracted beams, and that between the (0, 0) and (0, 1) order diffracted beams, must meet the condition $X + \lambda/\rho_i \} > 0$, where $i = X, Y$ and Ω represents the convergent angle of the focused beam (see Fig. 1). With the help of this inequality, we can estimate the overlap angle of the common-path region. For example, a common numerical aperture of 0.3 has an overlap angle of 10.6°. Such an overlap angle is much larger than those in the works of Lee et al. and Hsieh et al. [17, 18]. Based on the momentum conservation, the three-dimensional diffraction equations can be written as follows [22]:

$$k_{Xmn} = k_0 \sin\theta \cdot \cos\phi + \frac{2m\pi}{\rho_X}, \tag{1}$$

$$k_{Ymn} = k_0 \sin\phi + \frac{2n\pi}{\rho_Y}, \tag{2}$$

$$k_{Zmn} = \sqrt{k_0^2 - k_{Xmn}^2 - k_{Ymn}^2}, \tag{3}$$

where k_{Xmn} , k_{Ymn} , and k_{Zmn} are the X -, Y - and Z - components of the wavevector $\vec{k}_{mn}$ of the (m , n) order diffracted beam, ρ_X and ρ_Y are the grating pitches along the X - and Y - directions respectively, and $k_0 = 2\pi/\lambda$. The coordinate system of the three-dimensional diffraction is shown in Fig. 2. Note that the X - and Y -axes coincide with the grating vectors of a 2D grating scale for the 3D diffraction equations.

#190296 - $15.00 USD Received 5 Jun 2013; revised 4 Jul 2013; accepted 5 Jul 2013; published 1 Aug 2013
(C) 2013 OSA

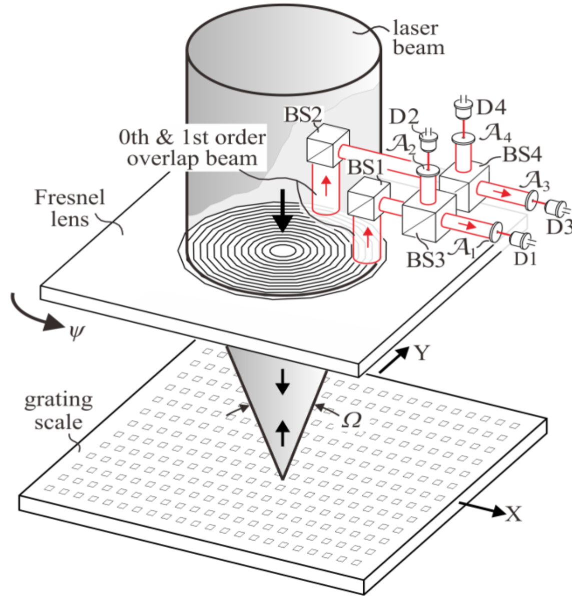

Fig. 1. The optical configuration of the CLPE.

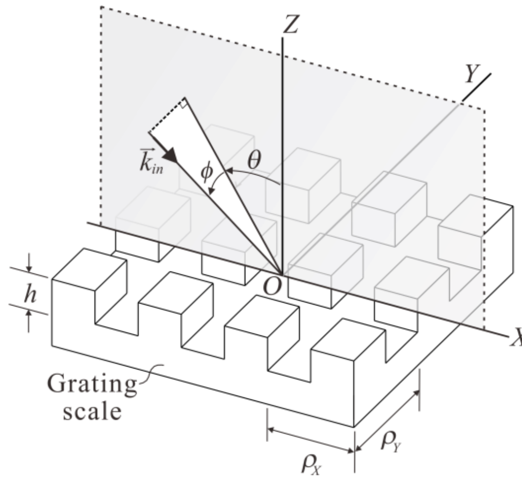

Fig. 2. Schematic of the coordinate system of the three-dimensional diffraction for a 2D grating scale. θ represents the angle of incidence for a wavevector $\vec{k}_{in}$ with respect to the Z -axis, and ϕ is the azimuth angle of the incidence plane with respect to the X -axis. ρ_X and ρ_Y are the grating pitches of a grating scale along the X - and Y - axes. O is the origin of the XYZ coordinate system. h is the grating depth.

2.1 Doppler frequency shift

The Doppler frequency shift carries the displacement information of the grating scale. In our previous work, we have shown that the Doppler frequency shift is the same within a specific order diffracted beam, whether the diffracted beam is focused or divergent along different incident directions [1]. Consider the 3-D diffraction of a two-dimensional sinusoidal surface relief grating scale with its two grating vectors respectively along the X - and the Y - axes. Such an arrangement of the sinusoidal grating scale can ensure that the maximum diffraction efficiencies for the (± 1, 0) and (0, ± 1) order diffracted beams, which lie respectively in the

#190296 - $15.00 USD Received 5 Jun 2013; revised 4 Jul 2013; accepted 5 Jul 2013; published 1 Aug 2013
(C) 2013 OSA

X - Z and the Y - Z planes [15]. In Fig. 1, after the diffracted beams return and pass again through the Fresnel lens, we can obtain three order diffracted beams, (0, 0), (1, 0), and (0, 1), which are collimated. We deliberately make the (0, 0) and the (1, 0) order diffracted beams, as well as the (0, 0) and the (0, 1) order diffracted beams, traverse partly in common-path. Two beam splitters, BS1 and BS2, are used to bend the common-path part of the (0, 0) and the (1, 0) order diffracted beams, as well as the common-path part of the (0, 0) and the (0, 1) order diffracted beams, to be directed to beam splitters, the BS3 and the BS4 respectively. These two common-path parts can respectively produce interference fringes that change with the displacement of the grating scale. The common-path part directed to the BS3 is split into two beams, which are measured respectively by photodetectors D1 and D2. Similarly, the common-path part directed to the BS4 is split into two beams, which are measured respectively by photodetectors D3 and D4. Assume that the optical read-head of the CLPE moves at a velocity $\vec{v} = v_X \hat{e}_X + v_Y \hat{e}_Y$, where $\hat{e}_X$ and $\hat{e}_Y$ are the unit vectors of the X - and Y - axes respectively. The frequency shift $\Delta\omega_1$ induced by a relative displacement between the grating scale and the readhead can be represented as follows [23]:

$$\Delta\omega_1 = \left(\vec{k}_{10} - \vec{k}_{in}\right) \cdot \vec{v} = \frac{2\pi v_X}{\rho_X}. \tag{4}$$

Similarly, the frequency shift $\Delta\omega_2$ induced by a relative displacement between the grating scale and the readhead can be represented as follows:

$$\Delta\omega_2 = \left(\vec{k}_{01} - \vec{k}_{in}\right) \cdot \vec{v} = \frac{2\pi v_Y}{\rho_Y} \tag{5}$$

From Eqs. (4) and (5), the Doppler frequency shifts $\Delta\omega_1$ and $\Delta\omega_2$, depend only on the velocity components v_X and v_Y respectively. We can see that the D1 and D2 are in charge of the measurement of the displacement along the X -axis, and the D3 and D4 are in charge of the measurement of the displacement along the Y -axis. The measurements of the X - and Y - displacement are essentially decoupled for the CLPE. Note that Eqs. (4) and (5) hold for runout and runoutless cases. Even for a runout case, the Doppler frequency shifts are decoupled between the X - and Y - displacements.

2.2 Two-aperture phase shifting technique

In our previous work, we adopted a pair of rectangular apertures to implement the phase shift [1]. Here, we adopt a pair of circular apertures, $\mathcal{A}_1$ and $\mathcal{A}_2$, to produce a specific phase shift between the signals measured respectively by the D1 and the D2. Similarly, we adopt a pair of circular apertures, $\mathcal{A}_3$ and $\mathcal{A}_4$, to produce a specific phase shift between the signals measured respectively by the D3 and the D4. Note that the mathematical manipulation of the circular aperture is more difficult than that of the rectangular aperture. Figure 3 shows a schematic of the two-aperture phase shifting technique. The intensities I_1 and I_2, measured respectively by the D1 and the D2, can be represented as follows:

$$I_1 \propto DC_1 + AC_1 \cos\left(\Delta\omega_1 t - \frac{\pi a}{q}\right), \tag{6}$$

$$I_2 \propto DC_2 + AC_2 \cos\left(\Delta\omega_1 t - \frac{\pi(a + 2\Delta)}{q}\right), \tag{7}$$

#190296 - $15.00 USD Received 5 Jun 2013; revised 4 Jul 2013; accepted 5 Jul 2013; published 1 Aug 2013
(C) 2013 OSA

where Δ is the spatial shift between the aperture $\mathcal{A}_1$ and the aperture $\mathcal{A}_2$ in the fringe space. Similarly, the intensities I_3 and I_4, measured respectively by the D3 and the D4, can be represented as follows:

$$I_3 \propto DC_3 + AC_3 \cos\left(\Delta\omega_2 t - \frac{\pi a}{q}\right), \tag{8}$$

$$I_4 \propto DC_4 + AC_4 \cos\left(\Delta\omega_2 t - \frac{\pi(a+2\Delta')}{q}\right), \tag{9}$$

where Δ' is the spatial shift between the aperture $\mathcal{A}_3$ and the aperture $\mathcal{A}_4$ in the fringe space. We can deliberately align the apertures to attain $2\Delta/q = (2\alpha-1)/2$ and $2\Delta'/q = (2\beta-1)/2$, where α and β are integers. These two conditions can be easily met by fine-tuning Δ and Δ' based on the Lissajous trace of I_1 and I_2 signals, as well as that of I_3 and I_4. Accordingly, we can have a phase shift of $\pi/2$ between I_1 and I_2, as well as between I_3 and I_4.

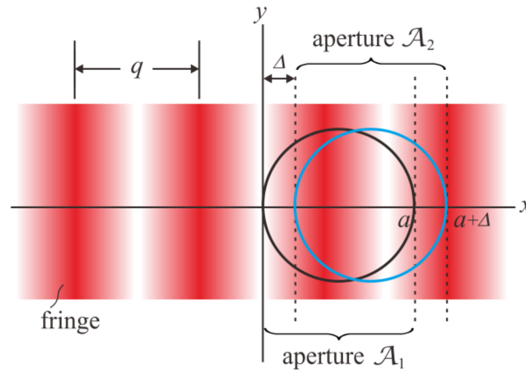

Fig. 3. Schematic of two-aperture phase shifting technique. a is the diameter of the circular apertures . Δ is the spatial shift between the aperture $\mathcal{A}_1$ and the aperture $\mathcal{A}_2$ in the fringe space.

Note that the spatial domain of the aperture $\mathcal{A}_1$ and the aperture $\mathcal{A}_2$ is different from that of the aperture $\mathcal{A}_3$ and the aperture $\mathcal{A}_4$. The common phase term in Eqs. (6) and (7), as well as in Eqs. (8) and (9), a/q, can be removed in the phase unwrapping and the displacement calculation because the CPLE is an incremental type laser encoder. Thus, the CLPE can also realize the phase shifting after the reference beam interferes with the test beam for common-path interferometers, just like the CPLE in our previous work [1]. Substituting Eqs. (4) and (5) into Eqs. (7) and (9), we can have the relationship between the grating displacement ΔX along the X-axis and the measured phase change $\Delta\Phi_X$, as well as that between the grating displacement ΔY along the Y-axis and the measured phase change $\Delta\Phi_Y$, as the following expressions:

$$\Delta X = \frac{\rho_X}{2\pi}\Delta\Phi_X, \tag{10}$$

#190296 - $15.00 USD Received 5 Jun 2013; revised 4 Jul 2013; accepted 5 Jul 2013; published 1 Aug 2013
(C) 2013 OSA

$$\Delta Y = \frac{\rho_Y}{2\pi}\Delta\Phi_Y. \tag{11}$$

Equations (10) and (11) show that the grating displacement depends on the grating pitch and phase change. They also show that the grating displaces a pitch distance for a full cycle of the quadrature signal for the grating displacements along the X - and the Y -axes.

3. Runout tolerance analysis

A planar encoder has only three types of runout: yaw, tilt, and standoff. These three types of runout come from the runout tolerance of the moving stage. The tolerances for a common stage are typically near 5 arc-sec (2.4×10^{-5} rad) and 0.4 μm for yaw/tilt and standoff tolerances [24]. The works of Kao et al. [15, 25] adopted the configuration with the 2D grating scale as a movable component. Physically, the runout of the grating scale may make the coordinate system of the 2D grating scale not coincide with the coordinate system of the grating velocity. Thus, a coordinate transformation must be considered in their analysis, and the displacement measurements along the X - and Y - axes do couple to each other for their planar encoder. For the CLPE, we adopt the configuration with the optical read-head of the CLPE as a moveable component. As the coordinate systems of the moveable optical read-head and the 2D grating scale always coincide, the CLPE can attain a decoupling 2D displacement measurement between the displacements along the X - and Y - axes. In the following, we will apply the first-order analysis to estimate runout tolerance of the CLPE.

First, consider a case of yaw runout at ψ angle for the CLPE (see Fig. 1). The interference fringe will have a displacement with respect to the apertures, $\mathcal{A}_1$, $\mathcal{A}_2$, $\mathcal{A}_3$, and $\mathcal{A}_4$. We can estimate the yaw runout tolerance based on the following inequality:

$$\frac{D}{2}\cdot\psi \le \frac{q}{10000}, \tag{12}$$

where D is the diameter of the laser beam (see Fig. 1). Note that the factor of 10,000 can ensure the displacement error from runout smaller than (a grating pitch)/10,000. As q and D are about 2.5 mm and 10 mm respectively, we can have the estimated yaw runout tolerance near 5×10^{-5} rad (10.3 arc-sec). Such a yaw runout tolerance is enough and ensures a displacement measurement error within 0.16 nm (if the grating pitch $\rho_X = \rho_Y = 1.6$ μm).

Second, consider a case of tilt runout for the CLPE. As the effects of the X -tilt and the Y -tilt of the CLPE are the same, we can consider X -tilt only; that is, θ = 0° and $\varphi = \tau$. The interference fringe will have a displacement with respect to the apertures $\mathcal{A}_1$, $\mathcal{A}_2$, $\mathcal{A}_3$, and $\mathcal{A}_4$. We can estimate the tilt runout tolerance based on the following inequality:

$$\frac{1}{2}\cos^{-1}\left(\frac{\vec{k}_{10}\cdot\vec{k}_{10}^{//}}{\sqrt{\vec{k}_{10}\cdot\vec{k}_{10}}\sqrt{\vec{k}_{10}^{//}\cdot\vec{k}_{10}^{//}}}\right)\sqrt{\left(\frac{D}{2}\right)^2+f^2} \le \frac{q}{10000}, \tag{13}$$

where $\vec{k}_{10}^{//}$ represents the projection vector of $\vec{k}_{10}$ in the X - Z plane, and f is the focal length of the Fresnel lens. Similarly, we adopt the same factor of 10,000 as Eq. (12). As q, D and f are about 2.5 mm, 10 mm, and 16.67 mm respectively, we can obtain the estimated tilt runout tolerance $\tau \cong 2.87\times10^{-5}$ rad (5.93 arc-sec). Such a tilt runout tolerance is enough and ensures a displacement measurement error smaller than 0.16 nm (if the grating pitch $\rho_X = \rho_Y = 1.6$ μm).

#190296 - $15.00 USD Received 5 Jun 2013; revised 4 Jul 2013; accepted 5 Jul 2013; published 1 Aug 2013
(C) 2013 OSA

Third, consider a case of standoff runout at S μm for the CLPE. The depth of focus for a common lens with the f-number of 1.67 is about 3.5 μm [26]. Such a depth of focus is much larger than the standoff runout of the stage. Thus, the standoff tolerance for the CLPE is S = 3.5 μm, and standoff runout within such a tolerance cannot induce additional measurement error for the CLPE.

4. Experiments and results

Figure 4 shows the schematic of the experimental setup in this study with the CLPE configuration built in the readhead. A frequency-stabilized He-Ne laser source (model HRS015, Thorlabs, Inc.) with a wavelength of 632.991 nm (in vacuum) was used to provide a good light source. Since the CLPE is common-path in its configuration, a low coherence light source, such as a diode laser, can be used for compactness. A 2D grating scale (manufactured by Taiwan Mask Corp.) with grating pitches of 1.6 μm had two grating vectors coinciding respectively with the X - and Y - axes. The dimensions of the grating scale were 100 mm × 100 mm. The grating scale was mounted on an optical table (model: RS4000- 412 −12, Newport Inc.). The substrate of the grating was borosilicate glass with a thermal expansion coefficient of $3.3\times10^{-6}/^{\circ}\mathrm{C}$. To provide long- and small-range 2D displacements, a 2D composite stage was made of two types of 2D linear stages: two long-ranged motorized linear stages (model: SGSP26-200, Sigma Inc.) with a controller (model: SHOT-702, Sigma Inc.) and a small-ranged piezoelectric stage (model: Tritor 100 SG, Piezosystem Jena) with a controller (model: NV40/3 CLE, Piezosystem Jena). The small-range piezoelectric stage used three embedded strain gauges as its displacement sensors [27]. The CPLE was used to measure the displacement of the 2D composite-stage.

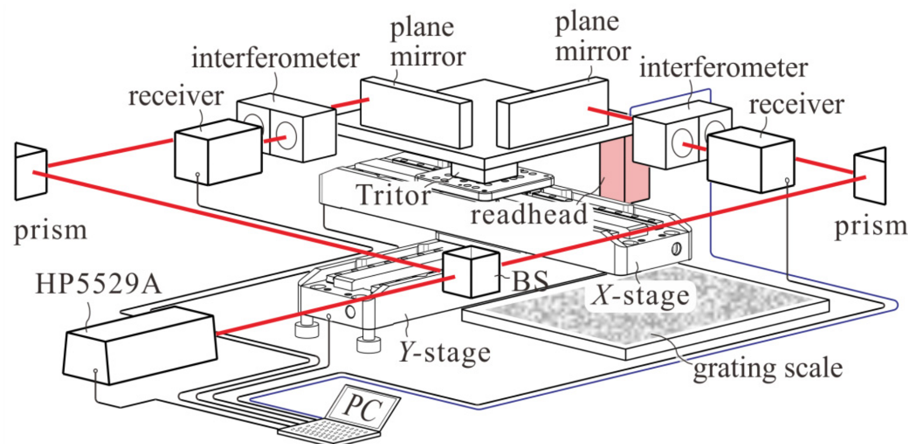

Fig. 4. Schematic of experimental setup with the CLPE configuration built in the readhead.

4.1 Long-range measurement

The long-range measurement results of the HP5529A and the CLPE in a square path with each side at 8 mm are shown in Fig. 5. The results of the HP5529A and the CLPE match well. At corners of the square path, there exist about 50-nm discrepancies between the result of the HP5529A and the CLPE. As such discrepancies fall to near 10 nm at the starting position of the stage, we infer that such discrepancies come mainly from the cosine error between the measurement axes of the HP5529A and the CLPE. Certainly, the drift effect contributes to these discrepancies. The drift issue will be discussed in section 4.3, where we address stability.

#190296 - $15.00 USD Received 5 Jun 2013; revised 4 Jul 2013; accepted 5 Jul 2013; published 1 Aug 2013
(C) 2013 OSA

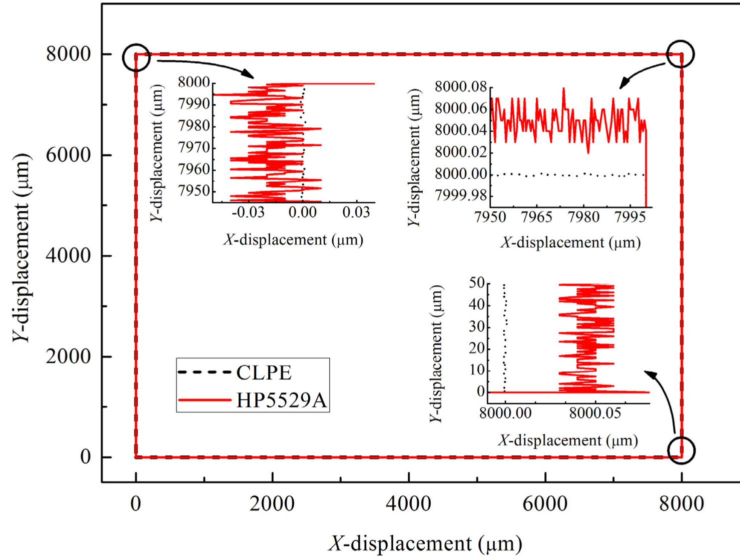

Fig. 5. Results of 8-mm square path movement by the HP5529A and the CLPE.

4.2 Short-range measurement

(i) 20-μm triangular movement

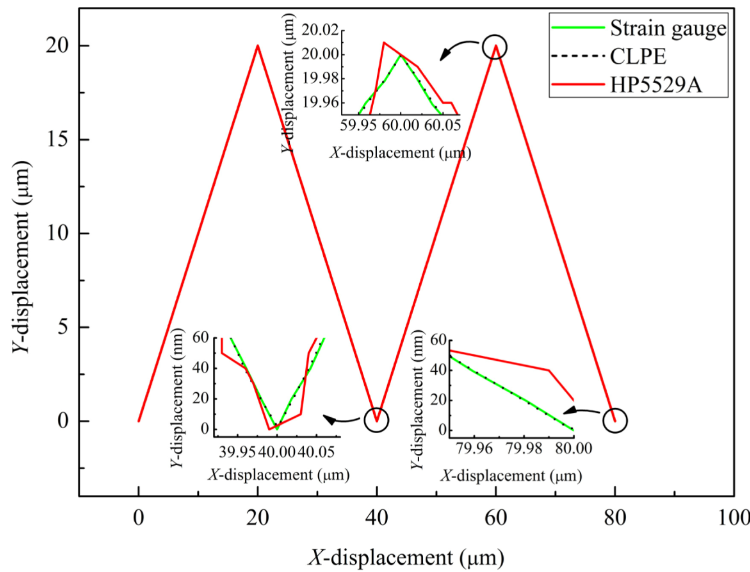

Fig. 6. Results of 20-μm triangular path movement by the HP5529A, the CLPE, and the strain gauge.

Figure 6 demonstrates the results of 20-μm triangular path movement by the HP5529A, the CLPE, and the strain gauge built in the piezoelectric stage. These three results match well. Three insets of Fig. 6 show details of the discrepancies between the three methods. From these insets, we can find a larger difference in the result of the HP5529A from those of the CLPE and the strain gauge. Such a difference comes mainly from the resolution truncation of the HP5529A (10-nm resolution).

#190296 - $15.00 USD Received 5 Jun 2013; revised 4 Jul 2013; accepted 5 Jul 2013; published 1 Aug 2013
(C) 2013 OSA

(ii) 10-nm diameter circular movement

In order to investigate the short-range measurement capability of the CLPE, we drove the piezoelectric stage using two analog voltage inputs to move the stage in a circular path with a diameter of 10 nm under the open-loop mode. Figure 7 represents the results of 10-nm diameter circular movement by the CLPE and the strain gauge built into the piezoelectric stage. These two results have good matching in the trend. However, the data scatter of the strain gauge has a much larger range than that of the CLPE. Such a data scatter comes from the resolution limit of the strain gauge (about 3 nm). In contrast, the CLPE has a subnanometric resolution and a promising potential for subnanometric applications. Due to high-frequency noise, the dashed line of the CLPE looks like a "black bold" line. The resolution of the CLPE will be discussed in section 5.2.

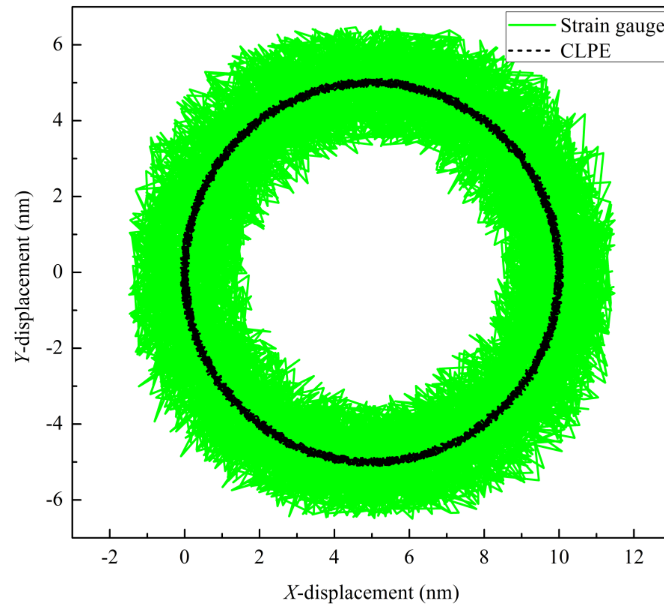

Fig. 7. Results of 10-nm diameter circular movement by the strain gauge and the CLPE.

4.3 Stability measurement

Stability is an important specification to a common-path laser encoder or grating interferometer. To verify the system stability of the CLPE, which reflects its immunity to environmental disturbances, we immobilized both the coarse and fine stages carrying the grating scale for three hours. The two drivers of the composite stage were turned off electrically. We used the CLPE and the HP5529A to simultaneously monitor the X - and Y - displacement variations of the grating scale. Figure 8 shows the system stability measurement results of the CLPE and the HP5529A for three hours. We've deliberately shifted the HP5529A data by −500 nm for convenient observation. Results show that the CLPE data had stabilities of −0.59 ± 0.43 nm/h and −0.63 ± 0.47 nm/h respectively in the X - and Y - axes, which were over two orders of magnitude smaller than those indicated by the HP5529A data (−118.67 ± 49.50 nm/h and −120 ± 50.00 nm/h respectively). The CLPE data physically reflected the state of the still stage. The insets of Fig. 8 show the X - and Y - data of the CLPE from 5400 s to 5508 s. In addition, the system drift data of the CLPE in the X - and Y - direction were two orders of magnitude smaller than those of the HP5529A within three hours.

#190296 - $15.00 USD Received 5 Jun 2013; revised 4 Jul 2013; accepted 5 Jul 2013; published 1 Aug 2013
(C) 2013 OSA

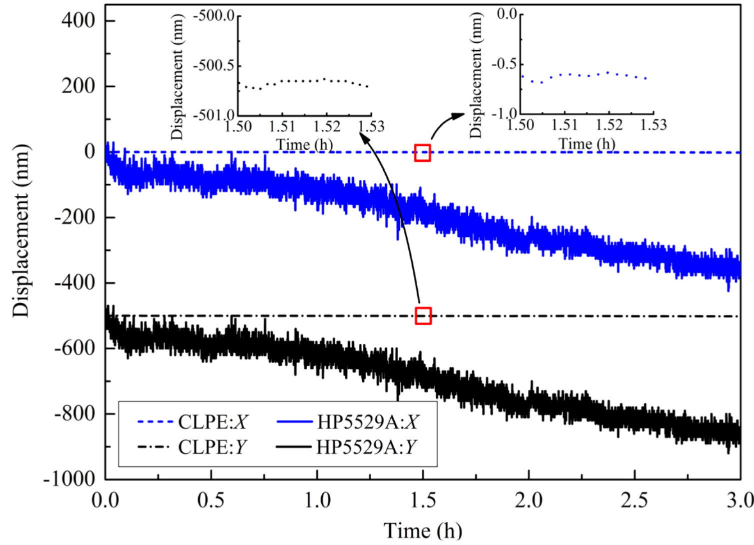

Fig. 8. System stability measurement results of the CLPE and the HP5529A for three hours.

5. Discussion

5.1 Quadrature error

Generally speaking, quadrature error comes from DC offset, AC amplitude variation, and phase error. Actually, the drift effect and the optics nonlinearity also appear as a quadrature error [2, 21, 28]. We adopted the same approach in our previous work to correct the output signals of the CLPE [21]. Assume two raw CLPE signals represented by data points p, $I_i(p)$ and $i = 1, 2, 3, 4$, which are measured respectively by the D1, D2, D3 and D4. If 1000 data points are sampled and saved in an array in the register in every quadrature period, we can calculate the maximum and minimum values of the 1000-point data array. Thus we can have $I_i'(p)$ without DC offset and amplitude variation as follows:

$$I_i'(p) = \frac{I_i(p) - \{\max[I_i(p)] + \min[I_i(p)]\}/2}{\{\max[I_i(p)] - \min[I_i(p)]\}/2}, \; i = 1, 2, 3, 4, \qquad (14)$$

where the functions max[ ] and min [ ] respectively calculate the maximum and minimum values of a data array. As for the periodic error from the phase error, it can be effectively removed or minimized by carefully aligning apertures of the CLPE.

5.2 Resolution

The common concept of the displacement resolution is the smallest measurement increment “between different measurement states”. Consider a measured object keeping motionless. One can adopt a laser interferometer with a resolution specification of 10 nm to monitor the motionless state of the object. Theoretically, it is expected that the readout should be zero. However, the readout may usually be much larger than tens of nanometers for the motionless object. Can we still say that the resolution of the laser interferometer is 10 nm? If yes, how can we explain the displacement variation of the motionless object? We all know that such a phenomenon comes from the environmental disturbances and then the noise. If we adopt the same view point of the resolution as the laserscale BL-57 (Sony Precision Technology) and our previous works [1, 21, 29], this question can have a reasonable answer. Note that there is

#190296 - $15.00 USD Received 5 Jun 2013; revised 4 Jul 2013; accepted 5 Jul 2013; published 1 Aug 2013
(C) 2013 OSA

no international standard on the resolution. In the following, we will adopt the same approach in our previous work [1] to estimate the measurement resolution of the CLPE.

In Eqs. (10) and (11), two measured phases suffer from various high- and low-frequency noises. Though the CLPE has a theoretical displacement measurement resolution of about 24 pm for grating pitches of 1.6 μm, these noises spoil the measurement resolutions. Because the stage is held still ($d\left(\Delta\Phi_X\right) = d\left(\Delta\Phi_Y\right) = 0$), the effect of the grating pitch variations or pitch tolerances on the measurement error can be dropped. That is, the results in Fig. 8 indicate only the phase noises. We can estimate the measurement resolution of the CLPE using the stability data [21]. The measurement times for all short- and long-range experiments in this study were within 600 s. A review of every 600-s time interval in Fig. 8 shows two estimated measurement resolutions of 0.23 ± 0.074 nm and 0.25 ± 0.080 nm, respectively, in the X - and Y - axes. For short-range measurement, the review time interval can be as low as 60 s, and two greatly superior estimated measurement resolutions of 0.07 ± 0.021 nm and 0.07 ± 0.023 nm in the X - and Y - axes can be obtained. In contrast, the drift of the HP5529A is large, so the corresponding estimated measurement resolutions respectively in the X - and Y - axes within 600 s are 130.0 ± 18.6 nm and 130.7 ± 18.6 nm, and within 60 s are 80.85 ± 16.61 nm and 82.01 ± 16.36 nm, respectively. The major difference of estimated resolutions between the CLPE and the HP5529A comes from the drift effect. Although the HP5529A has a resolution of 10 nm listed on its data sheet, practically, we cannot attain such a resolution in a common engineering environment, since the drift effect engulfs the resolving capability of the HP5529A. Note that the resolution of a laser encoder or an interferometer is not a constant value and depends on the measurement time interval, since drift exists.

6. Conclusion

We propose an innovative CLPE for 2D displacement measurement. As the CLPE is common-path, it can effectively overcome the environmental disturbance. The CLPE adopts a 1-x telescope configuration, so its runout tolerances are large enough to cope with the problem of practical runout. An analysis method for runout tolerances of the CLPE is presented. We verify the performance of the CLPE for short- and long-range measurements. The experimental results demonstrate that the CLPE not only can measure 2D displacement with high resolutions of 0.07 ± 0.021 nm and 0.07 ± 0.023 nm in the X - and Y - axes (for a short time interval of 60 s), but also presents high system stabilities of –0.59 ± 0.43 nm/h and –0.63 ± 0.47 nm/h respectively in the X - and Y - axes.

Acknowledgments

This study was supported by the National Science Council of Taiwan under contracts NSC 100-2628-E-032- 001- and NSC 102-2221-E-032-012-MY3. The authors cordially thank Prof. C.-K. Lee of National Taiwan University for his assistance.